



1 A one-dimensional temperature and age modeling study for selecting the 2 drill site of the oldest ice core around Dome Fuji, Antarctica

3
4 Takashi Obase¹, Ayako Abe-Ouchi^{1,2}, Fuyuki Saito³, Shun Tsutaki^{2,4}, Shuji Fujita^{2,4}, Kenji
5 Kawamura^{2,3,4} and Hideaki Motoyama^{2,4}

6 ¹ Atmosphere and Ocean Research Institute, The University of Tokyo, Kashiwa, Japan

7 ² National Institute of Polar Research, Research Organization of Information and Systems, Tachikawa, Japan

8 ³ Japan Agency for Marine-Earth Science and Technology (JAMSTEC), Yokosuka, Japan

9 ⁴ The Graduate University for Advanced Studies, SOKENDAI, Tachikawa, Japan

10 *Correspondence to:* Takashi Obase (obase@aori.u-tokyo.ac.jp)

11 **Abstract.** The recovery of a new Antarctic ice core spanning the last ~1.5 million years will advance
12 our understanding of climate system dynamics during the Quaternary. Recent glaciological field
13 surveys have been conducted to select the most suitable core location near Dome Fuji (DF), Antarctica.
14 Specifically, ground-based radar-echo soundings have been used to acquire highly detailed images of
15 bedrock topography and internal ice layers. In this study, we use a one-dimensional (1-D) ice flow
16 model to compute the temporal evolutions of age and temperature, in which the ice flow is linked with
17 not only transient climate forcing associated with past glacial–interglacial cycles, but also transient
18 basal melting diagnosed along the evolving temperature profile. We investigated the influence of ice
19 thickness, accumulation rate, and geothermal heat flux on the age and temperature profiles. The model
20 was constrained by the observed temperature and age profiles reconstructed from DF ice-core analysis.
21 The results of sensitivity experiments indicate that ice thickness is the most crucial parameter
22 influencing the computed age of the ice because it is critical to the history of basal temperature and
23 basal melting, which can eliminate old ice. The 1-D model was applied to a 54 km long transect in the
24 vicinity of DF and compared with radargram data. We found that the basal age of the ice is mostly
25 controlled by the local ice thickness, demonstrating the importance of high spatial resolution surveys
26 of bedrock topography for selecting ice-core drilling sites.

27 1. Introduction

28 Earth's climate system experienced glacial–interglacial cycles during the Quaternary,
29 associated with the waxing and waning of continental ice sheets and climate system feedbacks. Ice
30 cores from the Antarctic ice sheet have provided fruitful information on climate system changes in the
31 past because they can provide continuous reconstructions of past atmospheric compositions and
32 temperature up to ~800 thousand years before the present (ka BP) (Jouzel et al., 2007; Kawamura et
33 al., 2017). Such reconstructions have contributed to our understanding of the climate system dynamics
34 of glacial–interglacial cycles (e.g., Abe-Ouchi et al. 2013; Obase et al. 2021). Meanwhile, a stacked
35 sequence of marine sediments (Lisiecki and Raymo 2005) indicates that the periodicity of glacial–
36 interglacial cycles changed from 40 to 100 ka at the middle Pleistocene transition (MPT, approximately
37 800–1250 ka BP, Paillard, 2001; Clark et al., 2006). However, continuous ice core records that cover
38 the MPT are still lacking, leading to a limited understanding of the mechanisms of this climate event.
39 To help remedy this issue, the International Partnership for Ice Core Sciences (IPICS) has identified
40 the quest for an “oldest ice core” as a critically scientific challenges. In this article, we define the term
41 “old ice” as a continuous ice core with a basal age reaching 1.5 million years (Ma) BP, as defined in a
42 IPICS community paper (Fischer et al., 2013).

43 In recent years, international efforts have been made to find plausible sites to obtain old ice
44 in several locations in the interior of the Antarctic continent. In particular, in EPICA (European Project
45 for Ice Coring in Antarctica) Dome C (EDC), glaciological surveys and ice-flow modeling studies
46 have been used to select the location of the suitable sites (Parrenin et al., 2017; Young et al., 2017;



48 Passalacqua et al., 2018; Lilien et al., 2021). The present article focuses on Dome Fuji (DF), Antarctica,
49 which is located at 77.31° S, 39.70° E, with a surface elevation of 3810 m above sea level, and ice
50 thickness of 3028 m. The most recent ice core at DF was obtained between 2003 and 2006 (Motoyama
51 et al., 2021). The ice age at the bottom of this core was approximately 720 ka BP based on Antarctic
52 ice core chronology 2012 (AICC2012) (Kawamura et al., 2017; Uemura et al., 2018). The temperature
53 of the ice was at the pressure-melting point near the bedrock (Motoyama et al., 2021). Recently, field
54 surveys have been conducted to collect bedrock elevation data near DF using ground and airborne
55 radar surveys. On the basis of surveys performed by Japanese Antarctic Research Expeditions (JARE)
56 since the late 1980s until 2008, the results of which are included in BEDMAP2 datasets (Fretwell et
57 al., 2013), the typical ice thickness around DF is approximately 2000–3200 m (Fig. 1). Later, the 54th
58 JARE (2012–2013 Antarctic summer) conducted ground-based radar surveys in areas where subglacial
59 mountains were detected in the south of DF (data compiled in Tsutaki et al., 2022). More recently,
60 Alfred Wegener Institute (AWI) in Germany conducted airborne radar surveys covering the DF area
61 (Karlsson et al., 2018). Based on these data, the 59th and 60th JARE (2017–2018 and 2018–2019
62 Antarctic summers) conducted ground radar surveys to investigate the internal layers of ice sheets over
63 an areal extent of ~ 50 km, covering DF and NDF sites (77.8° S, 39.05° E) (Rodríguez-Morales et al.,
64 2020).

65 To select suitable ice-core drilling sites, it is essential to investigate the conditions required to
66 preserve old ice using constraints from glaciological and climatological data. Previous ice-flow
67 modeling studies have examined the requirements to preserve old ice using both three-dimensional (3-
68 D) and one-dimensional (1-D) models. Pattyn (2010) used a 3-D ice sheet model under present-day
69 constant climate forcing, and suggested the importance of minimal horizontal flow and low geothermal
70 heat flux (GHF) to preserve old ice near the base of ice sheets. Other studies have used 3-D models to
71 represent 3-D ice-flow fields and ice age for the relatively small area near Antarctic Domes
72 (Huybrechts et al., 2007; Seddik et al., 2011; Sun et al., 2014; Passalacqua et al., 2018; Zhao et al.,
73 2018). These studies estimated the age distribution of the ice expected from 3-D ice flow fields under
74 a constant present-day climate. More recent studies used glacial–interglacial cycle forcing (Sutter et
75 al., 2019, 2021) and discussed how the past variation of the Antarctic ice sheet affects ice age
76 distributions.

77 One-dimensional vertical ice-flow models have been used as the vertical profiles of age and
78 temperature near Antarctic Domes, where horizontal flow is relatively minor. Horizontal velocity in
79 the vicinity of DF and NDF is $< 2 \text{ m a}^{-1}$, evidenced by satellite-based measurements (Rignot et al.,
80 2011, 2017; Mouginit et al., 2012). Such 1-D models perform well in long-term forward simulations
81 over glacial cycles and are able to conduct many experiments with different parameters. In particular,
82 Fischer et al. (2013) investigated the influence of a wide range of parameters, including ice thickness,
83 accumulation, and GHF on the basal age of ice. The key finding was that melting at the base reduces
84 the likelihood of old ice; hence, a lower accumulation rate and ice thickness compared with previous
85 ice core sites are required conditions to avoid basal melting and preserve old ice. Other studies used
86 an equivalent 1-D ice-flow model, investigated the necessary conditions to keep the ice base frozen
87 (Van Liefferinge and Pattyn, 2013; Van Liefferinge et al., 2018), and examined the observed basal
88 conditions of the ice (Passalacqua et al., 2017). Parrenin et al. (2017) estimated ice-flow parameters
89 and basal melting rate using internal layers of the ice near EDC and proposed candidate sites for old
90 ice. Saito et al. (2020) presented a numerical scheme of ice advection calculation and conducted
91 numerical simulations using idealized glacial cycle forcings. This contributed to a good representation
92 of annual layer thickness, which is critical to the occurrence of old ice near the base of the ice column.

93 Simplified factors in previous modeling studies were the time-dependent climate forcing and
94 temperature profile, which are critical to basal ice melting. In particular, the basal temperature of the
95 ice sheet shows a minimum during interglacials because it takes a long time to convey the information
96 of surface temperature changes to the base of the ice sheet (Saito and Abe-Ouchi 2004; Van Liefferinge
97 et al., 2018). In this context, the model used in Parrenin et al. (2007, 2017) assumed that basal melting



98 rates were constant over time, and Fischer et al. (2013) used a constant climate forcing. Some studies
99 (Van Liefferinge and Pattyn 2013; Passalacqua 2017; Van Liefferinge et al., 2018) have investigated
100 ice temperature using realistic climate forcing, but did not investigate the resultant impact on the age
101 of the ice. Similarly, Hondoh et al. (2002) and Talalay et al. (2021) estimated GHF at DF and other
102 Antarctic domes based on observed vertical temperature profiles, but the observed age–depth profiles
103 were not used as constraints.

104 Despite the close link between the temperature and age of ice owing to basal melting, the
105 thermodynamics of ice and time-dependent basal melting were not represented in previous modeling
106 studies of old ice. In this study, we use a 1-D ice-flow model, which simultaneously computes the
107 evolution of ice temperature and age, and the model is forced by past climate history. The remainder
108 of the article is organized as follows: Section 2 describes the 1-D model used in this study. In Sect. 3,
109 we apply this model to DF and conduct systematic sensitivity experiments to calibrate GHF and a
110 tuning parameter of the vertical profile of ice velocity by comparing simulated age and temperature
111 profiles with observations. We also use parameters at EDC to examine whether the model can simulate
112 temperature and age profiles under different glaciological conditions. In Sect. 4, using the results of
113 the tuned vertical velocity parameters, we investigate the influences of ice thickness, surface mass
114 balance (SMB), and GHF on the basal temperature and age. In Sect. 5, we apply the 1-D model to the
115 DF–NDF transect and compare the results with the internal layers of the ice.

116 2. Method

117 2.1. Model description

118 We used a 1-D ice-flow model, IcIES-2 (Saito et al., 2020). This model computes the temporal
119 evolutions of the age and temperature profiles of ice columns.

120 The evolution of the age of the ice is computed using the vertical advection equation,
121

$$122 \frac{\partial A}{\partial t} = -w \frac{\partial A}{\partial z} + 1. \quad (1)$$

123 where A is the age of the ice, defined as the duration since deposition, and w is the vertical velocity of
124 the ice (a positive value indicates upward velocity). Here, ζ is a normalized coordinate defined as $\zeta =$
125 $\frac{s}{H}$ where s is the surface elevation, z is the height above bedrock, and H is the ice thickness (thus $\zeta =$
126 1 and 0 correspond to the ice surface and base, respectively). The first and second terms on the right-
127 hand side of Equation (1) represent the vertical advection and aging owing to time-lapse, respectively.

128 The vertical velocity of the ice can be represented as:

$$129 w(\zeta) = - \left[\left(M_s + M_b - \frac{\partial H}{\partial t} \right) \omega(\zeta) - M_b \right]. \quad (2)$$

130 The terms M_s and M_b represent surface (positive indicates ice gain) and basal (positive indicates ice
131 melt) mass balance caused by accumulation and ablation, respectively, and $\frac{\partial H}{\partial t}$ is the change in ice
132 thickness over time. The normalized vertical velocity profile, ω , is given as a function of the
133 normalized coordinate following previous studies (Van Liefferinge and Pattyn, 2013; Passalacqua et
134 al., 2017; Van Liefferinge et al., 2018), and derived from Lliboutury (1979):

$$135 \omega(\zeta) = 1 - \frac{p+2}{p+1} (1 - \zeta) + \frac{1}{p+1} (1 - \zeta)^{p+2}. \quad (3)$$

136 where ω is 1 at the surface and 0 at the base. Hence, if we assume steady state, $\frac{\partial H}{\partial t} = 0$, the vertical
137 velocity of the ice at the surface and base equates to $-M_s$ and M_b , respectively. The shape of ω with
138 different p parameters is shown in Fig. 2, indicating that a larger p -value tends to induce a larger
139 downward ice velocity. Compared with Fischer et al. (2013), in the case of $m = 0.5$ in their study (Fig.
140 2 dashed lines), $p = 3$ from Equation (3) gives a different vertical temperature profile, with a smaller
141 vertical velocity, particularly near the base of the ice.

142 The temperature of the ice is computed using the following vertical advection and diffusion
143 equation:



144
$$\frac{\partial T}{\partial t} = -w \frac{\partial T}{\partial z} + \frac{1}{\rho_I c_p} \frac{\partial}{\partial z} \left(\kappa \frac{\partial T}{\partial z} \right). \quad (4)$$

145 where κ is the thermal conductivity, ρ_I is the ice density, and c_p is the heat capacity of the ice. The
146 strain heating term is neglected in the present study. The thermal conductivity and specific heat
147 capacity of the ice are functions of temperature (Greve and Blatter 2009, following Ritz, 1987). The
148 density of ice is set as a constant (910 kg m^{-3}), i.e. we ignore effects of lower density in the firn column.

149 Boundary conditions at the surface and base of the ice are required to close the equations. At
150 the ice surface, the age is set as 0, assuming no surface melt, and the temperature is set to the surface
151 temperature at the given time. The basal boundary conditions for temperature depend on the basal
152 condition:

153
$$\frac{\partial T}{\partial z} \Big|_b = -\frac{G}{\kappa} \text{ if no melting, } (5)$$

154
$$T_b = T_{pm} \text{ if melting, } (6)$$

155 where G is the GHF at the ice–bedrock boundary, and T_{pm} is the pressure-melting point of the ice,
156 which is given as a function of depth using a Clausius–Clapeyron gradient ($8.7 \times 10^{-4} \text{ K m}^{-1}$). The
157 basal melting rate at the ice–bedrock interface is determined by the conservation of heat:

158
$$M_b \rho_I L = G - \kappa \frac{\partial T}{\partial z} \Big|_b, \quad (7)$$

159 where L is the latent heat of the ice ($335,000 \text{ J kg}^{-1}$), and $\frac{\partial T}{\partial z} \Big|_b$ is the temperature gradient at the ice–
160 bedrock interface. This model assumes basal melting only occurs at ice–bedrock interfaces, and the
161 temperature gradient at the ice–bedrock interface is calculated using a central difference discretization.
162 The calculated basal melting rate M_b influences the velocity field according to Equation (2). Basal
163 melting can occur in the interior of the ice as represented by polythermal ice sheet models, but we
164 ignore such effects in this study for simplicity. For this reason, we set the vertical resolution of the
165 model for thermodynamics as relatively coarse ($\sim 30 \text{ m}$) to prevent representing layers of basal melting,
166 which can have significant errors in the diagnosis of basal melting rates.

167 We adopted different vertical resolution setups in computations of the temperature and age of
168 the ice. The ice profile was discretized with 101 even vertical layers for thermodynamics; it was
169 discretized with 2661 unevenly spaced vertical layers (finer near the base to resolve the thin layers of
170 old ice) for age calculations, which was optimized following Saito et al. (2020). In the typical ice
171 column thickness of 3000 m near DF, the vertical resolution was set to approximately 20 m near the
172 surface and 20 cm near the bedrock, which is sufficient to resolve paleoclimate information (glacial–
173 interglacial annual layer variations) of $\sim 1 \text{ ka}$. We used the rational function-based constrained
174 interpolation profile (RCIP) scheme in the advection equation for the numerical scheme, as in Saito et
175 al. (2020). One significant advantage of this scheme is the avoidance of numerical diffusion and ability
176 to reasonably preserve the time derivative of age, which is critical to the resolution of old ice. The time
177 step was set to 5 years, and the basal melting rates were updated every 500 years to reduce the effect
178 of temporal oscillations in basal melting and freezing.

179

180 **3. Model calibration using DF age and temperature profiles**

181 **3.1. Experimental design**

182 This section applies the 1-D model to DF under a realistic climate history for model calibration
183 and parameter constraints. Parrenin et al. (2007) determined the p -value as ~ 3.7 for DF, but the
184 chronology of ice older than 335 ka BP was not established at that time; therefore, we revisited DF to
185 determine the p -value covering the entire DF ice core age–depth dataset. The glaciological boundary
186 conditions at DF are summarized in Table 1: we used an ice thickness of 3028 m, a present-day SMB
187 of 30 ice equivalent mm a^{-1} (equivalent to 27.3 freshwater mm a^{-1} , based on Kameda et al., 2008 and
188 Fujita et al., 2011) and $-55.5 \text{ }^\circ\text{C}$ for the mean ice surface temperature at present. We determined the
189 boundary condition of ice surface temperature by calibrating the temperature profile to be consistent
190 with measured temperature profiles of the top 500 m within uncertainty ranges of the observations.



191 The observed present-day 10-m-depth annual mean snow temperature is -57.3 °C (Kameda et al.,
192 1997), which was also used in Parrenin et al. (2007). We note that the annual mean surface air
193 temperature based on meteorological observation was -54.4 °C (during the period 1995–1997,
194 Yamanouchi et al., 2003).

195 The model was forced by a realistic history of SAT (surface air temperature) and SMB. We
196 used local SAT anomalies at DF for the past 715 ka BP (Uemura et al., 2018) and the benthic record
197 of marine oxygen isotope data (Lisiecki and Raymo, 2005) to construct a continuous time series of
198 SAT anomalies during the last 2 Ma. We applied a simple translation of $\delta^{18}\text{O}$ to scale the temperature
199 change at DF by the amplitude of glacial–interglacial cycles:

$$200 \Delta T_s = \alpha(\beta - \delta^{18}\text{O}) \quad (8)$$

201 where $\delta^{18}\text{O}$ is the benthic marine oxygen isotope value [‰]; we set $\alpha = 4.5$, and $\beta = 3.23$
202 to scale the amplitude of the glacial cycles, which generated a time series of temperature change over
203 the last 2 Ma, as shown in Fig. 3a. We used past SMB as a function of temperature anomaly compared
204 with the present day following Huybrechts and Oerlemans (1990), as used in paleoclimate 3-D
205 Antarctic ice sheet modeling (Saito and Abe-Ouchi 2010). From this function, an increase in surface
206 air temperature of 1 °C increases SMB by approximately 7%. At the Last Glacial Maximum (LGM,
207 approximately 20 ka BP), when SAT was 8 °C cooler, the SMB was approximately 60% of the present
208 day (Fig. 3b), which is consistent with reconstructions based on the isotopic content of the ice (Parrenin
209 et al., 2016). This relationship between SAT and precipitation changes used in this study was within
210 uncertainties estimated from observations and climate model simulations, following a summary by
211 IPCC AR6 in Chapter 9.4.2.3 (Fox-Kemper et al. 2021), which used the studies of Bracegirdle et al.
212 (2020) and Frieler et al. (2015). Although this relationship is not based on SMB, but rather on
213 precipitation, herein we assume the precipitation change ratio is the same as that of the SMB. The other
214 boundary conditions (ice thickness and GHF) were set as constants in the present study. Some
215 modeling studies have considered ice thickness changes over glacial cycles because it can change by
216 approximately 200 m (Parrenin et al., 2007), but herein, the ice thickness is fixed, and the ice thickness
217 tendency is assumed to be 0. One recent study (Buizert et al., 2021) proposed that the temperature
218 change at the LGM in interior regions of the East Antarctic ice sheet was less than previously estimated.
219 Therefore, we conducted one set of experiments where SAT anomalies were set to 0%, 25%, 50%, and
220 75% of the standard experiments, while keeping changes in SMB the same. Furthermore, we also
221 applied this model to the conditions at EDC to check whether the model could simulate observed
222 temperature and age profiles (Table 1).

223 Using this set of boundary conditions, we conducted simulations with different p -values (1–
224 5) and GHFs (50 – 60 mW m^{-2}) to calibrate the model with observed values at the DF ice core. We used
225 the depth–age profile of the DF ice core, which was constructed by orbital tuning of a gas record above
226 ~ 2500 m, and by matching to the AICC2012 chronology below that depth (Kawamura et al., 2017).
227 We also used the measured depth–temperature profiles from the JARE54 surveys during the 2012–
228 2013 Antarctic summer (Buizert et al. 2021). The model was initialized with the conditions of 2 Ma
229 BP, where the initial age and temperature were set to 0 years and -10 °C for the entire ice column,
230 respectively. All experiments were integrated for 2 Ma to reach the present day; therefore, the age of
231 any ice older than 2 Ma did not appear in the experiments. These simplified initial conditions generated
232 unrealistic temperature fields in the early stage of the simulation, but realistic glacial cycle forcing
233 prevailed over the entire ice column within approximately 100 ka. Therefore, we mainly analyzed the
234 results of the last 1.5 Ma, which is sufficient to discuss old ice in this study.

235

| Parameters | DF | EDC |
|---|---------|----------|
| Ice thickness [m] | 3028 | 3233 |
| Surface mass balance [ice equivalent mm a^{-1}] | 30.0 | 28.4 |
| Surface temperature [°C] | -55.5 | -54.65 |

236 **Table 1:** List of parameters used in Sect. 3. Ice thickness (DF and EDC), surface mass balance, and



237 surface temperature at EDC come from Parrenin et al. (2007); surface mass balance at DF comes from
238 Kameda et al. (2008) and Fujita et al. (2011); surface temperature at DF is calibrated in this study but
239 is within previously observed ranges (Kameda et al., 1997; Yamanouchi et al., 2003).

240

241 3.2. Results for DF

242 In Fig. 4, the simulated temperature profiles at 0 ka (end of the simulations) with different
243 GHFs under the same p -value ($p = 3$) are compared with observations (Fig. 4a). The close-up of the
244 bottom 120 m of the ice column is shown in Fig. 4b; the basal temperature is well below melting point
245 with a GHF of 52 mW m^{-2} , and at the melting point with a GHF $> 56 \text{ mW m}^{-2}$. Compared with the
246 observed temperature profile (Fig. 4 black lines), the simulated temperature near the ice base was
247 colder by approximately $1 \text{ }^\circ\text{C}$. In all simulations, the simulated temperature profiles were generally
248 colder than observed temperature profiles especially in the middle of the ice columns (Fig. 4a).

249 The time series of simulated basal ice melting rates over the last 500 ka show that there have
250 been significant temporal changes in these rates over time (Fig. 5). With a GHF of 52 mW m^{-2} , the
251 temperature at the ice base has been below the melting point through the last 500 ka. In contrast, in the
252 case of a GHF of 55 mW m^{-2} , the basal melting rate is zero at 0 ka, while the maximum basal melting
253 rate of 1 mm a^{-1} occurs at the end of interglacial periods (e.g., 100 ka BP). This variability in basal
254 melting rate is caused by glacial–cycle forcing in SAT and SMB, and minimum basal melting tends to
255 occur in the interglacial periods. This result is broadly consistent with previous studies (Saito and Abe-
256 Ouchi, 2004; Van Liefferinge et al., 2018), in that colder ice, which accumulated during glacial
257 maximums, increased advection towards the ice base owing to an increased SMB during interglacials.
258 A larger GHFs (58 or 60 mW m^{-2}) results in basal melting occurring most of the time, with a rate of
259 approximately 3 mm a^{-1} . A downward flow of ice caused by basal melting (as in Equation 2)
260 compensates for the basal melting owing to the increased downward advection.

261 The simulated age profiles at the present day are compared with the reconstructed profiles in
262 Fig. 6a. With a small GHF (52 mW m^{-2}) where basal melting does not occur, the ice age at the ice–
263 bedrock interface is $> 1.5 \text{ Ma}$. In contrast, if basal melting occurs, the ice age at the ice–bedrock
264 interface can be much younger; for example, it is 980 or 650 ka for a GHF of 55 or 56 mW m^{-2} ,
265 respectively. The result obtained with a GHF of 55 mW m^{-2} exhibits the closest fit to the data at least
266 250 m above the bedrock. A larger GHF tends to decrease the ice age, owing to a higher basal melting
267 rate. In this article, we define the “resolution of age” (ka m^{-1}) as the inverse of annual layer thickness
268 as an indicator of old ice (Lilien et al., 2021). In Fig. 6b, the resolution of old ice is compared with the
269 actual DF ice core. The model results largely reproduced the glacial–interglacial contrasts in annual
270 layer thickness caused by the temporal variations of SMB at the site. The observed resolution of age
271 is approximately $0.5\text{--}1 \text{ ka m}^{-1}$ near the base, and the results using a GHF of 55 mW m^{-2} reproduced
272 similar values. Furthermore, on the basis of Fig. 6b, the annual layer thickness of 1.5 Ma BP ice is
273 approximately 0.1 mm if the ice base temperature is well below the melting point (dark blue lines).

274 In accordance with the results described above, a larger GHF tends to result in a higher basal
275 melting rate and younger age of ice at the base of the column. One critical point is that an excessive
276 GHF (i.e., an increase of the order of 2 mW m^{-2}) can have a considerable effect on the age of the ice
277 and the likelihood of old ice. Next, we evaluate the effects of different vertical velocity profiles. In
278 Figs 7 and 8, results with GHF of 55 mW m^{-2} and different p -values are compared. Generally, a larger
279 p -value induces a colder temperature (Fig. 7a) and a lower basal melting rate (Fig. 7b). The simulated
280 age profiles indicate that a larger p -value induces a younger age of ice in the mid-depths of the ice
281 column (Fig. 8). Both of these results can be explained by differences in advection, in that a larger p -
282 value induces larger advection of the temperature and age. Near the ice surface, the influence of basal
283 melting is relatively small; therefore, a larger vertical velocity tends to result in a younger ice age. In
284 contrast, near the base, a larger p -value results in a colder basal temperature owing to greater advection
285 of cold ice, which leads to less basal melting and an older ice age.

286



287 3.3. Results for EDC

288 We also applied this model to the EDC conditions to enable performance checks with one
289 different location. We used the parameters listed in Table 2 and conducted sensitivity experiments with
290 different GHFs. For the vertical velocity profile, we used $p = 2.3$ following Parrenin et al. (2007). The
291 model generally results in colder temperatures compared with observations, similar to DF (Fig. 9). The
292 results using a GHF of 51 mW m^{-2} give a basal ice age of approximately 900 ka (Fig. 10a), which is
293 close to the value (802 ka) presented in Veres et al. (2013), and the resolution of age closely fits the
294 chronology estimated from ice-core analysis (Fig. 10b). One important result is that the threshold of
295 GHF that allows basal melting is 5 mW m^{-2} lower at EDC than at DF. This result is generally consistent
296 with previous studies (Parrenin et al., 2007; Van Liefferinge et al., 2018). This lower threshold of GHF
297 can be attributed to the combination of larger ice thickness, smaller SMB, and higher SAT at the
298 present day. The results from the application to EDC show that our model produces results which are
299 consistent with observations for slightly different glaciological parameters.

301 3.4. Sensitivity of temperature amplitudes over glacial cycles

302 The results using DF conditions with different amplitude of temperature changes but the same
303 GHF and p parameters (same as Sect. 3.2) are summarized in Fig. 11, in terms of temperature and
304 basal melting rates. The control experiments exhibit colder ice temperatures near the middle of the ice
305 column than observations, and this cold bias can be reduced if a smaller temperature amplitude over
306 the glacial cycles is used (Fig. 11a), broadly consistent with Buizert et al. (2021). Temperature
307 amplitude also changes basal melting rates; a smaller amplitude of the glacial cycle contributes to
308 larger basal melting rates (Fig. 11b), because mean temperature over the glacial cycles increases if we
309 reduce a smaller temperature amplitude of glacial–interglacial cycles. The results using a fixed surface
310 temperature ($dTs = 0.0$) correspond to the same present-day SAT for the last 2 Ma, which induces basal
311 melting of $\sim 3 \text{ mm a}^{-1}$ most of the time. A slight fluctuation in basal melting still occurs owing to time-
312 dependent SMB. It is possible to tune the GHF as in Sect. 3.2, assuming different temperature changes
313 over the glacial cycle. We regard this as an uncertainty in the forcing, and we note that it can change
314 basal melting rates.

316 3.5. Summary of Sect. 3

317 On the basis of the results described in this section, we conclude that using a combination of p
318 $= 3$ and $\text{GHF} = 55 \text{ mW m}^{-2}$ gives reasonable temperature and age profiles; therefore, we decided to
319 use these values as calibrated parameters for the DF region. We use these parameters as a calibrated
320 values for the DF region for the following reasons. Later in the article, we investigate the possibility
321 of old ice in the DF region using different parameters (i.e., spatially variable ice thickness and GHF).
322 Hence, obtaining precise tuning at one specific DF location is unnecessary. We do not state that the
323 GHF of 55 mW m^{-2} is a single best estimate for the DF location compared to the previous estimates
324 (Burton-Johnson et al., 2020; Talalay et al., 2021), because there were assumptions in the vertical
325 velocity profiles and experimental design of this study. Also, the calibrated GHF depends on chosen
326 SAT scenario over the glacial cycles.

328 4. Sensitivity studies using various parameters around DF

329 4.1. Experimental design

330 This section investigates the impact of the other three parameters, ice thickness, SMB, and
331 GHF, which may have spatial variations in the DF region. We investigated a range of ice thicknesses
332 between 2000 and 3200 m, based on an ice thickness map of the area around DF (Fig. 1). We used
333 present-day SMB ranges of $25\text{--}35 \text{ ice mm a}^{-1}$. There is large uncertainty in GHF; we adopted a range
334 of $50\text{--}70 \text{ mW m}^{-2}$. The list of experiments is given in Table 2. Other aspects of the experimental design
335 are the same as in Sect. 3.

336



| Variable | Parameter range |
|--|----------------------|
| Ice thickness [m] | 2000–3200, every 100 |
| Present-day SMB [ice equivalent mm a ⁻¹] | 25–35, every 1 |
| GHF [mW m ⁻²] | 50–70, every 2 |

Table 2: List of experiments in Sect. 4.

4.2. Results

In Fig. 12a, the relative effects of ice thickness and GHF on basal temperature are compared, using the same SMB (30 mm a⁻¹). As in Sect. 3, we used an ice thickness of 3028 m, which is comparable to that at DF, and a threshold of GHF for basal melting of 55 mW m⁻². On the basis of the gradient of contours in Fig. 12a, an increase in ice thickness by 100 m has a comparable impact on the basal temperature as does an increase in GHF by 2 mW m⁻². In Fig. 12b, the relative effects of ice thickness and SMB are compared using the same GHF (55 mW m⁻²). A larger SMB results in a colder temperature; a 10% change in GHF leads to a ~4 °C change in the basal temperature, while a 10% change in SMB leads to a ~1 °C change. These results are generally consistent with those by Fischer et al. (2013). We note that the spatial distribution of SMB has a minor impact on the basal temperature compared with that of the ice thickness.

We further investigated the impact of different ice thicknesses on age profiles using climatic conditions at DF (SMB = 30 ice mm a⁻¹) and a calibrated GHF (55 mW m⁻²). Figure 13a shows the simulated age of the ice at 50 and 100 m above the ice–bedrock interface, which were used as indicator depths for potential sites by Fischer et al. (2013). The results indicate that the rate of aging of ice rapidly decreases with depth between 2900 and 3100 m owing to the occurrence of basal melting. Note that the age of 2 Ma BP is the limit of the experiments, and the results indicate that the old ice exists 50 m above the bedrock if the ice thickness is thicker than ~2100 m. Figure 13b shows the age resolution of the 1.5 Ma BP ice, indicating that a larger ice thickness tends to show a finer age resolution. The vertical age profiles and resolution of ice ages at three selected ice thicknesses (2200, 2600, and 3000 m) with the same GHG are shown in Fig. 14. The expected age resolution is approximately 10–20 ka m⁻¹.

5. Application to the DF–NDF transects

5.1. Experimental design

In this section, we apply the 1-D model to interpret the internal layers of the ice near DF, the structure of which was obtained by ground surveys during JARE59 (2017–2018). Here, we use the dataset from 17th December, 2017, which comprises a 54 km long transect from DF to NDF (Fig. 1). The horizontal axis of Fig. 15 indicates the distance from DF, and the vertical axis indicates the depth from the surface. The gray shading indicates the reflectivity, which is an indicator of contours representing ice of the same age. The bedrock elevation, shown by brown lines, was detected based on the maximum reflectivity from the base (Tsutaki et al., 2022). The bedrock elevation was calibrated to match the observed bedrock elevation at DF. We calculated the 1-D age and temperature profiles of the ice at approximately 400 m intervals along the transect. We assumed that the vertical profile of vertical velocity could be determined locally using Equation 1, and that there were no horizontal interactions in temperature and age in this simulation. The present-day SMB was linearly interpolated between DF (30 ice equivalent mm a⁻¹) and NDF (25.5 ice equivalent mm a⁻¹). As there was very limited information regarding the spatial distribution of GHF, we set a uniform value of 55 mW m⁻² following the discussion in Sect. 3. As described in Sect. 3, the initial age of the ice was set to 0, the temperature set to –10 °C, and the model was integrated over the last 2 Ma of forcing until it reached the present day (Fig. 3).

5.2. Results

In Fig. 15, the computed vertical profiles of the age are overlaid on a radargram using seven



383 colored lines, and the simulated basal temperature is indicated by shading in the bottom panel. The
384 colored bar below the radargram indicates the simulated present-day basal temperature. The simulated
385 distribution of ice age captured large-scale features in the black–white contour lines derived from the
386 radargram signal (grayscale color in Fig. 15). The simulated age contours of 21 ka BP (approximately
387 500 m depth) and 128 ka BP (approximately 1500 m depth) can be traced from DF, although the
388 deepest layer corresponding to an age older than 300 ka BP is hard to see in this image. Where ice is
389 relatively thick (e.g., 20–25 km from DF), the simulated age of the ice at the ice–bedrock interface is
390 younger than 700 ka BP, while ice older than 1.5 Ma BP occurs where the ice is relatively thin. A
391 comparison of the simulated ice age and the radargram signal gives an opportunity to examine the
392 validity of the model results. For example, between 5 and 35 km from DF, the computed 128 ka BP
393 contour deviates to shallower levels by 150 m from the tracked layer for the age from the radar
394 measurements, suggesting that the model overestimates the age of the ice near the bedrock in such
395 locations.

396

397 6. Discussion

398 In this study, we used a 1-D ice-flow model, which computes the temporal evolution of age
399 and temperature profiles. We used glaciological conditions at DF to tune some unknown parameters
400 according to the observed temperature and age profiles. The results showed that the age profile is
401 sensitive to the choice of GHF, but one experiment using a specific combination of GHF and vertical
402 velocity profile exhibited reasonable temperature and age profiles (Figs 4 and 6). One important result
403 is that the melting rate at the base of ice exhibits temporal changes associated with glacial–interglacial
404 forcing. This is caused by relatively cold ice deposited during glacial periods being pushed towards
405 the bottom of the ice column by increased SMB and downward advection during interglacial periods,
406 as shown in previous studies (e.g., Van Liefferinge et al., 2018). This point is critical for preserving
407 old ice, in that the temperature should be well below the melting point of the ice at the present day
408 because basal melting rates during glacial periods can be much higher than that of present day (Fig. 5,
409 blue lines). Our sensitivity experiments highlighted the relative effects of ice thickness and GHF,
410 whereby a small GHF excess above the condition that induces basal melting can result in a considerable
411 reduction in the age of ice at the ice–bedrock interface (Fig. 6a). Below, we discuss the limitation of
412 the interpretations of our results, their relevance to previous ice-flow modeling studies, and uncertainty
413 factors.

414 On the basis of data presented in Fig. 6, the GHF of 55 mW m^{-2} sufficiently explains the
415 observed temperature and age–depth profiles of the DF ice core. However, there is considerable
416 uncertainty in the estimation of the actual GHF value at DF because of some simplifications in the
417 model experiments and limited representations in physics. One point of difference is that the model
418 tends to give a generally colder temperature profile compared with the observations (Fig. 4), which
419 suggests that the model overestimates the GHF threshold of basal freezing. One possible reason for
420 this difference is that the basal melting of ice can occur within a certain ice thickness; the extrapolation
421 of observed temperature profiles at DF and EDC (Figs 4 and 9, black lines) shows that the ice reaches
422 the pressure-melting point approximately 30 m above the bedrock. This feature cannot be simulated in
423 the model of the present study, which assumes that basal melting can only occur at the ice–bedrock
424 interface. These representations in the physics of basal melting can be improved by using enthalpy as
425 a state variable and adopting polythermal ice sheet models (e.g., Aschwanden et al., 2012). Another
426 important factor in the temperature profiles is the temperature anomaly over glacial cycles, as a smaller
427 glacial–interglacial temperature change tends to result in a warmer, more linear temperature profile
428 compared with the control experiment (Fig. 11a). The temperature change over the last glacial cycle
429 used in this study is based on deuterium and oxygen isotopes (Uemura et al., 2018), which exhibit an
430 LGM temperature anomaly of approximately $8 \text{ }^\circ\text{C}$ (Fig. 3a). A recent study proposed that the
431 temperature anomaly at the LGM at DF and EDC was about a half of the previous estimates based on
432 the observed temperature profiles and other independent methods (Buizert et al., 2021). This study is



433 in agreement with Buizert et al. (2021) in that our control experiment exhibits colder ice temperatures,
434 especially at mid-depth within the ice column, and a smaller temperature difference between glacial
435 and interglacial periods improves the modeled temperature profiles (Fig. 11a). If this is indeed the case,
436 the actual threshold of GHF value for the basal freezing should be lower than that used in the control
437 experiment.

438 We note that the simulated age of the ice depends on the shape of the vertical velocity profile
439 of the ice. The formulation of the present study has a smaller vertical velocity of the ice, especially
440 near the base, compared with that used in Fischer et al. (2013). Because the age of the ice is related to
441 the inverse of the vertical velocity, a different vertical velocity profile or a p parameter can lead to a
442 quantitatively different result. Moreover, vertical velocity profiles represented by a single p -value are
443 merely one assumption; this formulation is derived from a solution of an idealized ice-sheet
444 configuration (Liboutry, 1979), which may not be the case for realistic ice-sheet. For example, the
445 observed magnitude of layer thinning of the DF ice core exhibits a decreasing trend over the bottom
446 500 m (Fig. 6). According to analyses of the DF ice core (Azuma et al., 1999; Saruya et al., 2022) or
447 3-D ice sheet modeling (Seddik et al., 2011), deformation of the ice or flow regime towards the ice
448 bottom is complex. Thus we suggest that both horizontal and vertical ice flow should be complex as
449 well, which may be difficult to represent by using the current formulation of vertical velocity profiles.

450 We also note that the resolution of 1.5 Ma ice, one indicator of old ice, depends on ice thickness.
451 In particular, Lilien et al. (2021) presented similar 1-D ice-flow model results from BELDC (Beyond
452 EPICA Little Dome C, ice thickness of ~ 2750 m) constrained by radar internal layers and estimated
453 the resolution of 1.5 Ma ice as 19 ± 2 ka m^{-1} . In contrast, our results for EDC conditions have a
454 resolution of the ice (with a small enough GHF to keep the base of the ice frozen) have an ice age
455 resolution of approximately 10 ka m^{-1} (Fig. 10, dark blue lines), which is approximately half of that in
456 Lilien et al. (2021). This difference can be attributed to the combination of the model parameters, such
457 as ice thickness, p of the vertical velocity profile, or SMB history (3233 m and $p = 2.3$ in this study),
458 because the two studies adopted the same formulation of the vertical velocity profile. According to
459 Figs 13 and 14, a larger ice thickness leads to a better resolution of the ice age if the base of the ice is
460 frozen throughout time. Therefore, we speculate that the different ice thickness, p -value, or SMB
461 history in the Lilien et al. (2021) study (whose value ranges were not explicitly presented) may have
462 caused the difference in the age resolution of 1.5 Ma BP ice.

463 Application of the 1-D model to the transect between DF and NDF provides an opportunity to
464 examine the influence of spatially varying glaciological conditions (e.g., ice thickness and GHF) on
465 the age of the ice. The simulated age–depth distributions with constant GHF but different ice thickness
466 and SMB exhibit general agreement with observed internal layers (Fig. 15). One noticeable model–
467 data discrepancy occurs at 14–18 km from DF, where the simulated age contours of 128 ka BP are
468 ~ 150 m above the observed internal layers traced from DF. This model–data discrepancy indicates that
469 the effects of vertical or horizontal advection (Huybrechts et al., 2007; Sutter et al., 2021) or ice
470 thickness changes over glacial cycles (Saito et al., 2020) may have contributed to this difference.
471 Although the relative importance of the spatial distributions of GHF, SMB, and horizontal flow is
472 difficult to assess in the present study, we expect that future glaciological data constraints and model
473 developments will better constrain these uncertain parameters and the spatial distribution of old ice.
474 One recently published present-day SMB from the vicinity of the DF region exhibits spatial
475 variabilities reflecting surface topographical features (Van Liefferinge et al., 2021). On the basis of
476 systematic sensitivity experiments (Sect. 4), we have shown that the impact of SMB on the age of the
477 ice is relatively minor compared with that of ice thickness, but the small-scale features present in
478 internal layers of the ice can be improved by using the spatial distribution of present-day SMB, and
479 this will contribute to the selection of the most suitable drilling site.

480

481 7. Conclusions

482 We draw the following conclusions from this study.

483



- 483 1. In experiments using the configurations of DF, the model largely reproduced the observed age and
484 temperature profiles under a calibrated GHF. If the GHF is small enough to keep the basal
485 temperature below the melting point, it is expected that ~1.5 Ma could be present. If such old ice
486 exists, the simulated annual layer thickness of ~1.5 Ma BP ice is approximately ~0.1 mm, which
487 corresponds to 10 ka m⁻¹. According to IPICS, this is a feasible resolution for analysis with
488 minimized effects of diffusion. This is also true for EDC, but the threshold of GHF for basal
489 melting is different because of a different ice thickness and SMB.
- 490 2. Under the configuration and range of parameters of the present study, the ice thickness has a larger
491 impact on basal melting than does the present-day SMB; an ice thickness difference of ~100 m
492 corresponds to a SMB difference of 5 ice equivalent mm a⁻¹ (Fig. 12). Near the DF region, the ice
493 thickness has larger spatial variability above these ranges, while SMB does not. Though there is
494 considerable uncertainty in the spatial distribution of GHF, ice thickness is suggested to be one of
495 the most critical factors for the preservation of old ice.
- 496 3. The climate forcing of the past influences the temperature and age profiles, and induces a
497 substantial change in basal melting rates. The calibrated age profile at DF resulted from temporally
498 evolving basal melting rates, which mostly occurred after interglacial periods. This temporally
499 changing basal melting can eliminate the old ice of ~1.5 Ma BP.
- 500 4. From the simulation of the DF–NDF transect, a small ice thickness and colder basal temperature
501 are the necessary conditions for the presence of the old ice of ~1.5 Ma. However, a small ice
502 thickness contributes to a coarser resolution of the old ice (small annual layer thickness), which
503 may make it difficult to extract paleoclimate information. As discussed in Pattyn (2010), ice
504 thickness is found to be a compromising factor in the selection of a drilling site.
- 505 5. The simulation along the DF–NDF transect does not reproduce the depth of the internal layers of
506 the ice corresponding to 128 ka BP at some locations (e.g., at distances 5–35 km from DF),
507 suggesting possible error in the simulated age of ice near the bottom of the ice column. The
508 simulated age of ice in this area, especially where there is a large discrepancy between the
509 simulation and radar images, could be caused by uncertainties derived from several assumptions
510 or uncertainty in the model or methods, including spatial distributions of GHF, representation in
511 vertical temperature profile that depends only on normalized altitude (DF ice core suggests
512 complex ice-flow near its base), representation in thermodynamics associated with basal melting,
513 or history of surface temperature changes. Therefore, future improvements in numerical models
514 and methods would contribute to better constraining the age of the ice.

515 A recent compilation of ice thickness data around DF indicates the presence of complex and steep
516 terrain in the area, with uncertainty in bedrock elevation of > 60 m (Tsutaki et al., 2022), highlighting
517 the necessity of a high spatial resolution survey of bedrock topography. The results from this study
518 help to support the interpretation of observational data and the selection of a suitable drilling site.

519

520 **Code availability:**

521 The numerical model is available from Github. <https://github.com/saitofuyuki/icies2.git>

522

523 **Data availability:**

524 The scripts and data for conducting experiments and analyzing results are available at AORI-CESD
525 (<https://cesd.aori.u-tokyo.ac.jp/cesddb/publication/index.html>). All figures were generated using GMT
526 version 4.5.9. The ice core chronology and temperature at DF are available from previously published
527 articles (Veres et al., 2013; Kawamura et al., 2017; Buizert et al., 2021).

528

529 **Author contribution**

530 T. O., A. A-O, and F. S. conceived the study, developed the numerical model, designed and carried
531 out experiments, and analyzed the results. T. S., S. F., K. K., and H. M. provided glaciological data



532 from JARE surveys and contributed to the experimental design. T. O. prepared the manuscript with
533 contributions from all co-authors.

534

535 **Competing interests**

536 The authors declare that they have no conflict of interest.

537

538 **Acknowledgments**

539 We thank Kenichi Matsuoka, Brice Van Liefferinge, and Ralf Greve for their fruitful discussions. This
540 research was supported by JSPS Kakenhi JP17H06104, JP17H06323 and JP18H05294. T. O., A. A-
541 O, and F. S. were supported by JPJSBP120213203. F. S. was also supported by JSPS Kakenhi
542 JP17K05664. We thank David Wacey, PhD, from Edanz (<https://jp.edanz.com/ac>) for editing a draft
543 of this manuscript.

544

545 **References**

- 546 1. Abe-Ouchi, A., Saito, F., Kawamura, K., Raymo, M. E., Okuno, J., Takahashi, K., and Blatter, H.
547 Insolation-driven 100,000-year glacial cycles and hysteresis of ice-sheet volume. *Nature* 500,
548 190–193, doi: 10.1038/nature12374, 2013
- 549 2. Aschwanden, A., Bueler, E., Khroulev, C., and Blatter, H.: An enthalpy formulation for glaciers
550 and ice sheets, *J. Glaciol.*, 58, 441–457, doi:10.3189/2012JoG11J088, 2012.
- 551 3. Azuma, N., Wang, Y., Mori, K., Narita, H., Hondoh, T., Shoji, H., and Watanabe O.: Textures and
552 fabrics in the Dome F (Antarctica) ice core, *Ann. Glaciol.*, 29, 163–168,
553 <https://doi.org/10.3189/172756499781821148>, 1999.
- 554 4. Bracegirdle, T. J., Krinner, G., Tonelli, M., et al. Twenty first century changes in Antarctic and
555 Southern Ocean surface climate in CMIP6. *Atmos Sci Lett.*, doi: 10.1002/asl.984, 2020
- 556 5. Burton-Johnson, A., Dziadek, R., and Martin, C., Geothermal heat flow in Antarctica: current and
557 future directions, *The Cryosphere*, 14, 3843–3873, doi:10.5194/tc-14-3843-2020, 2020
- 558 6. Buizert, C., Fudge, T. J., Roberts, W. H., Steig, E. J., Sherriff-Tadano, S., Ritz, C., Lefebvre, E.,
559 Edwards, J., Kawamura, K., Oyabu, I., and Motoyama, H. et al.: Antarctic surface temperature
560 and elevation during the Last Glacial Maximum, *Science* 372(6546), 1097–1101, doi:
561 10.1126/science.abd2897, 2021
- 562 7. Clark, P., Archer, D., Pollard, D., Blum, J. D., Rial, J. A., Brovkin, V., Mix, A. C., Pisias, N. G.
563 and Roy, M.: The middle Pleistocene transition: characteristics, mechanisms, and implications for
564 long-term changes in atmospheric pCO₂, *Quaternary Science Reviews*, 25, 23–24, 3150–3184.
565 doi: 10.1016/j.quascirev.2006.07.008, 2006
- 566 8. Fischer, H., Severinghaus, J., Brook, E., Wolff, E., Albert, M., Alemany, O., Arthern, R., Bentley,
567 C., Blankenship, D., Chappellaz, J., Creyts, T., Dahl-Jensen, D., Dinn, M., Frezzotti, M., Fujita,
568 S., Gallee, H., Hindmarsh, R., Hudspeth, D., Jugie, G., Kawamura, K., Lipenkov, V., Miller, H.,
569 Mulvaney, R., Parrenin, F., Pattyn, F., Ritz, C., Schwander, J., Steinhage, D., van Ommen, T., and
570 Wilhelms, F.: Where to find 1.5 million yr old ice for the IPICS “Oldest-Ice” ice core, *Clim. Past*,
571 9, 2489–2505, doi:10.5194/cp-9-2489-2013, 2013.
- 572 9. Fox-Kemper, B., H. T. Hewitt, C. Xiao, G. Adalgeirsdottir, S. S. Drijfhout, T. L. Edwards, N. R.
573 Golledge, M. Hemer, R. E. Kopp, G. Krinner, A. Mix, D. Notz, S. Nowicki, I. S. Nurhati, L. Ruiz,
574 J-B. Sallee, A. B. A. Slangen, Y. Yu: Ocean, Cryosphere and Sea Level Change. In: *Climate*
575 *Change 2021: The Physical Science Basis. Contribution of Working Group I to the Sixth*
576 *Assessment Report of the Intergovernmental Panel on Climate Change [Masson-Delmotte, V., P.*
577 *Zhai, A. Pirani, S. L. Connors, C. Pean, S. Berger, N. Caud, Y. Chen, L. Goldfarb, M. I. Gomis,*
578 *M. Huang, K. Leitzell, E. Lonnoy, J.B.R. Matthews, T. K. Maycock, T. Waterfield, O. Yelekci,*
579 *R. Yu and B. Zhou (eds.)]. Cambridge University Press, 2021.*
- 580 10. Frieler, K., Clark, P., He, F. et al. Consistent evidence of increasing Antarctic accumulation with
581 warming. *Nature Clim Change* 5, 348–352. doi: 10.1038/nclimate2574, 2015.



- 582 11. Fretwell, P., Pritchard, H. D., Vaughan, D. G., Bamber, J. L., Barrand, N. E., Bell, R., Bianchi,
583 C., Bingham, R. G., Blankenship, D. D., Casassa, G., Catania, G., Callens, D., Conway, H., Cook,
584 A. J., Corr, H. F. J., Damaske, D., Damm, V., Ferraccioli, F., Forsberg, R., Fujita, S., Gim, Y.,
585 Gogineni, P., Griggs, J. A., Hindmarsh, R. C. A., Holmlund, P., Holt, J. W., Jacobel, R. W.,
586 Jenkins, A., Jokat, W., Jordan, T., King, E. C., Kohler, J., Krabill, W., Riger-Kusk, M., Langley,
587 K. A., Leitchenkov, G., Leuschen, C., Luyendyk, B. P., Matsuoka, K., Mouginot, J., Nitsche, F.
588 O., Nogi, Y., Nost, O. A., Popov, S. V., Rignot, E., Ripplin, D. M., Rivera, A., Roberts, J., Ross,
589 N., Siegert, M. J., Smith, A. M., Steinhage, D., Studinger, M., Sun, B., Tinto, B. K., Welch, B. C.,
590 Wilson, D., Young, D. A., Xiangbin, C., and Zirizzotti, A.: Bedmap2: improved ice bed, surface
591 and thickness datasets for Antarctica, *The Cryosphere*, 7, 375–393, doi: 10.5194/tc-7-375-2013,
592 2013.
- 593 12. Fujita, S., Holmlund, P., Andersson, I., Brown, I., Enomoto, H., Fujii, Y., Fujita, K., Fukui, K.,
594 Furukawa, T., Hansson, M., Hara, K., Hoshina, Y., Igarashi, M., Iizuka, Y., Imura, S., Ingvander,
595 S., Karlin, T., Motoyama, H., Nakazawa, F., Oerter, H., Sjöberg, L. E., Sugiyama, S., Surdyk, S.,
596 Ström, J., Uemura, R., and Wilhelms, F.: Spatial and temporal variability of snow accumulation
597 rate on the East Antarctic ice divide between Dome Fuji and EPICA DML, *The Cryosphere*, 5,
598 1057–1081, doi:10.5194/tc-5-1057-2011, 2011.
- 599 13. Greve, R., and Blatter, H. K.: *Dynamics of Ice Sheets and Glaciers*, Springer, Berlin, 2009.
- 600 14. Hondoh, T., Shoji, H., Watanabe, O., Salamatin, A. N., and Lipenkov, V. Y.: Depth-age and
601 temperature prediction at Dome Fuji station, East Antarctica, *Ann. Glaciol.*, 35, 384–390,
602 <https://doi.org/10.3189/172756402781817013>, 2002.
- 603 15. Huybrechts, P. and Oerlemans, J.: Response of the Antarctic ice sheet to future greenhouse
604 warming, *Climate Dynamics*, 5, 93–102, 1990.
- 605 16. Huybrechts, P., Rybak, O., Pattyn, F., Ruth, U., and Steinhage, D.: Ice thinning, upstream
606 advection, and non-climatic biases for the upper 89% of the EDML ice core from a nested model
607 of the Antarctic ice sheet, *Clim. Past*, 3, 577–589, <https://doi.org/10.5194/cp-3-577-2007>, 2007.
- 608 17. Jouzel, J., Masson-Delmotte, V., Cattani, O., Dreyfus, G., Falourd, S., Hoffmann, G., Minster, B.,
609 Nouet, J., Barnola, J. M., Chappellaz, J., Fischer, H., Gallet, J. C., Johnsen, S., Leuenberger, M.,
610 Loulergue, L., Luethi, D., Oerter, H., Parrenin, F., Raisbeck, G., Raynaud, D., Schilt, A.,
611 Schwander, J., Selmo, E., Souchez, R., Spahni, R., Stauffer, B., Steffensen, J. P., Stenni, B.,
612 Stocker, T. F., Tison, J. L., Werner, M., and Wolff, E. W.: Orbital and Millennial Antarctic Climate
613 Variability over the Past 800,000 Years, *Science*, 317, 793–796,
614 <https://doi.org/10.1126/science.1141038>, 2007.
- 615 18. Kameda, T., Azuma, N., Furukawa, T., Ageta, Y. and Takahashi, S.: Surface mass balance,
616 sublimation and snow temperatures at Dome Fuji Station, Antarctica, in 1995. *Proc. NIPR Symp.*
617 *Polar Meteorol. Glaciol.*, 11, 24–34, 1997
- 618 19. Kameda, T., Motoyama, H., Fujita, S., and Takahashi, S.: Temporal and spatial variability of
619 surface mass balance at Dome Fuji, East Antarctica, by the stake method from 1995 to 2006, *J.*
620 *Glaciol.*, 54, 107–116, doi:10.3189/002214308784409062, 2008.
- 621 20. Karlsson, N. B., Binder, T., Eagles, G., Helm, V., Pattyn, F., Van Liefferinge, B., and Eisen, O.:
622 Glaciological characteristics in the Dome Fuji region and new assessment for “Oldest Ice”, *The*
623 *Cryosphere*, 12, 2413–2424, doi:10.5194/tc-12-2413-2018, 2018.
- 624 21. Kawamura, K., Parrenin, F., Uemura, R., Vimeux, F., Severinghaus, J. P., Hutterli, M. A.,
625 Nakazawa, T., Aoki, S., Jouzel, J., Raymo, M. E., Matsumoto, K., Nakata, H., Motoyama, H.,
626 Fujita, S., Goto-Azuma, K., Fujii, Y., and Watanabe, O.: Northern Hemisphere forcing of climatic
627 cycles in Antarctica over the past 360,000 years *Nature*, 448, 912–917, doi:10.1038/nature06015,
628 2007.
- 629 22. Kawamura, K., Abe-Ouchi, A., Motoyama, H., Ageta, Y., Aoki, S., Azuma, N., Fujii, Y., Fujita,
630 K., Fujita, S., Fukui, K., Furukawa, T., Furusaki, A., Goto-Azuma, K., Greve, R., Hirabayashi,
631 M., Hondoh, T., Hori, A., Horikawa, S., Horiuchi, K., Igarashi, M., Iizuka, Y., Kameda, T., Kanda,



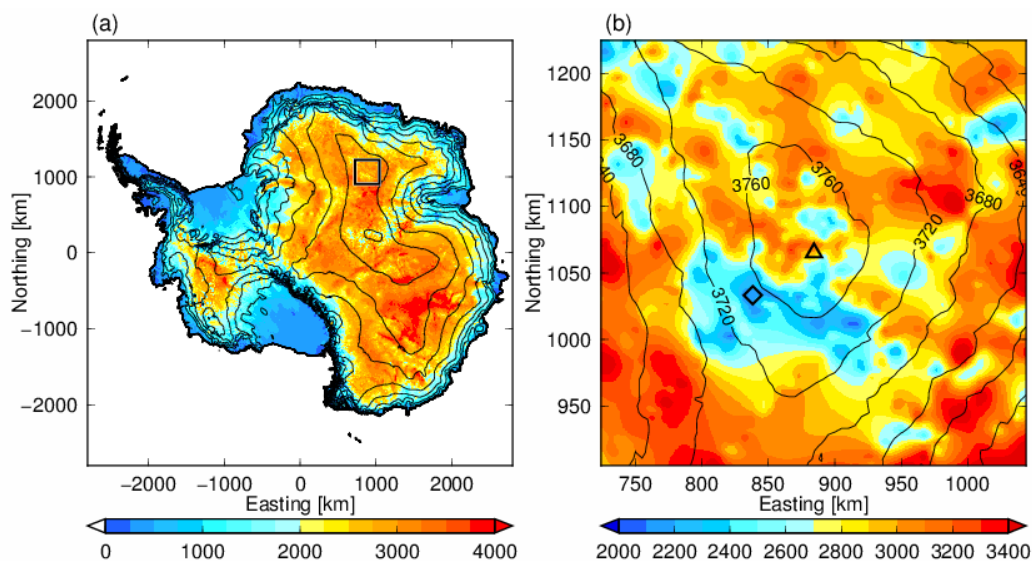
- 632 H., Kohno, M., Kuramoto, T., Matsushi, Y., Miyahara, M., Miyake, T., Miyamoto, A., Nagashima,
633 Y., Nakayama, Y., Nakazawa, T., Nakazawa, F., Nishio, F., Obinata, I., Ohgaito, R., Oka, A.,
634 Okuno, J., Okuyama, J., Oyabu, I., Parrenin, F., Pattyn, F., Saito, F., Saito, T., Saito, T., Sakurai,
635 T., Sasa, K., Seddik, H., Shibata, Y., Shinbori, K., Suzuki, K., Suzuki, T., Takahashi, A.,
636 Takahashi, K., Takahashi, S., Takata, M., Tanaka, Y., Uemura, R., Watanabe, G., Watanabe, O.,
637 Yamasaki, T., Yokoyama, K., Yoshimori, M., and Yoshimoto, T.: State dependence of climatic
638 instability over the past 720,000 years from Antarctic ice cores and climate modeling, *Sci. Adv.*,
639 3, 1–13, doi:10.1126/sciadv.1600446, 2017.
- 640 23. Lilien, D. A., Steinhage, D., Taylor, D., Parrenin, F., Ritz, C., Mulvaney, R., Martín, C., Yan, J.-
641 B., O'Neill, C., Frezzotti, M., Miller, H., Gogineni, P., Dahl-Jensen, D., and Eisen, O.: Brief
642 communication: New radar constraints support presence of ice older than 1.5 Myr at Little Dome
643 C, *The Cryosphere*, 15, 1881–1888, doi:10.5194/tc-15-1881-2021, 2021.
- 644 24. Lisiecki, L. E. and Raymo, M. E.: A Pliocene-Pleistocene stack of 57 globally distributed benthic
645 $\delta^{18}\text{O}$ records, *Paleoceanography*, 20, PA1003, doi:10.1029/2004PA001071, 2005
- 646 25. Liboutry, L.: A critical review of analytical approximate solutions for steady state velocities and
647 temperatures in cold ice-sheets, *Z. Gletscherkd. Glazialgeol.*, 15, 135–148, 1979
- 648 26. Motoyama H, Takahashi, A., Tanaka, Y., Shinbori, K., Miyahara, M., Yoshimoto, T., Fujii, Y.,
649 Furusaki, A., Azuma, N., Ozawa, Y., Kobayashi, K., and Yoshise, Y. : Deep ice core drilling to a
650 depth of 3035.22m at Dome Fuji, Antarctica in 2001–07. *Annals of Glaciology*, 62, 212–222,
651 doi:10.1017/aog.2020.84, 2021
- 652 27. Mouginot, J., B. Scheuchl, and E. Rignot: Mapping of Ice Motion in Antarctica Using Synthetic-
653 Aperture Radar Data, *Remote Sensing*, 4, 2753–2767. doi: 10.3390/rs4092753, 2012.
- 654 28. Obase, T., A. Abe-Ouchi, F. Saito: Abrupt climate changes in the last two deglaciations simulated
655 with different Northern ice sheet discharge and insolation, *Scientific Reports*, 11, doi:
656 10.1038/s41598-021-01651-2, 2021
- 657 29. Paillard, D. Glacial cycles: Toward a new paradigm, *Review of Geophysics*, 39, 3,
658 <https://doi.org/10.1029/2000RG000091>, 2001.
- 659 30. Pattyn, F.: Antarctic subglacial conditions inferred from a hybrid ice sheet/ice stream model,
660 *Earth. Planet. Sci. Let.*, 295, 451–461, doi:10.1016/j.epsl.2010.04.025, 2010.
- 661 31. Parrenin, F., Barnola, J.-M., Beer, J., Blunier, T., Castellano, E., Chappellaz, J., Dreyfus, G.,
662 Fischer, H., Fujita, S., Jouzel, J., Kawamura, K., Lemieux-Dudon, B., Loulergue, L., Masson-
663 Delmotte, V., Narcisi, B., Petit, J.-R., Raisbeck, G., Raynaud, D., Ruth, U., Schwander, J., Severi,
664 M., Spahni, R., Steffensen, J. P., Svensson, A., Udisti, R., Waelbroeck, C., and Wolff, E.: The
665 EDC3 chronology for the EPICA Dome C ice core, *Clim. Past*, 3, 485–497, doi:10.5194/cp-3-
666 485-2007, 2007.
- 667 32. Parrenin, F., Fujita, S., Abe-Ouchi, A., Kawamura, K., Masson-Delmotte, V., Motoyama, H.,
668 Saito, F., Severi, M., Stenni, B., Uemura, R., and Wolff, E.: Climate dependent contrast in surface
669 mass balance in East Antarctica over the past 216 ka, *J. Glaciol.*, 36, 455–466,
670 doi:10.1017/jog.2016.85, 2016.
- 671 33. Parrenin, F., Cavitte, M. G. P., Blankenship, D. D., Chappellaz, J., Fischer, H., Gagliardini, O.,
672 Masson-Delmotte, V., Passalacqua, O., Ritz, C., Roberts, J., Siegert, M. J., and Young, D. A.: Is
673 there 1.5-million-year-old ice near Dome C, Antarctica?, *The Cryosphere*, 11, 2427–2437, doi:
674 10.5194/tc-11-2427-2017, 2017.
- 675 34. Passalacqua, O., Ritz, C., Parrenin, F., Urbini, S., and Frezzotti, M.: Geothermal flux and basal
676 melt rate in the Dome C region inferred from radar reflectivity and heat modelling, *The*
677 *Cryosphere*, 11, 2231–2246, <https://doi.org/10.5194/tc-11-2231-2017>, 2017.
- 678 35. Passalacqua, O., Cavitte, M., Gagliardini, O., Gillet-Chaulet, F., Parrenin, F., Ritz, C., and Young,
679 D.: Brief communication: Candidate sites of 1.5 Myr old ice 37 km southwest of the Dome C
680 summit, East Antarctica, *The Cryosphere*, 12, 2167–2174, doi:10.5194/tc-12-2167-2018, 2018.
- 681 36. Rignot, E., J. Mouginot, and B. Scheuchl: Ice Flow of the Antarctic Ice Sheet, *Science*. 333. 1427-



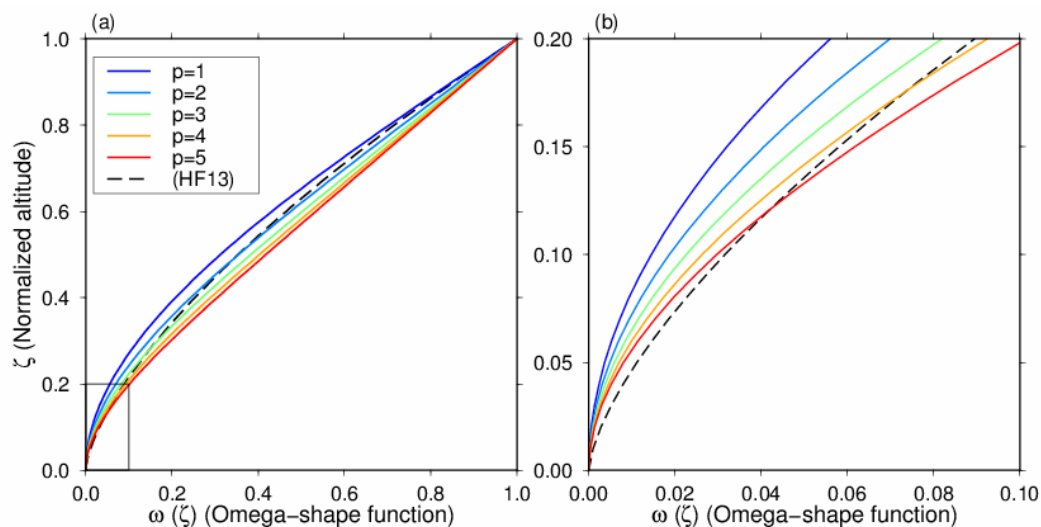
- 682 1430. doi: 10.1126/science.1208336, 2011.
- 683 37. Rignot, E., J. Mouginot, and B. Scheuchl: MEaSURES InSAR-Based Antarctica Ice Velocity Map,
684 Version 2. Boulder, Colorado USA. NASA National Snow and Ice Data Center Distributed Active
685 Archive Center. doi: 10.5067/D7GK8F5J8M8R, 2017.
- 686 38. Ritz, C.: Time dependent boundary conditions for calculation of temperature fields in ice sheets.
687 In: E. D. Waddington and J. S. Walder (Eds.), *The Physical Basis of Ice Sheet Modelling*, IAHS
688 Publication No. 170, pp. 207-216. IAHS Press, Wallingford, UK, 1987.
- 689 39. Rodrigez-Morales, F. Braaten, D., Mai, H. T., Paden, J., Gogineni, P., Yan, J-B., Abe-Ouchi, A.,
690 Fujita, S., Kawamura, K., Tsutaki, S., Van Liefferinge, B., Matsuoka, K., and Steinhage, D.: A
691 Mobile, Multi-Channel, UWB Radar for Potential Ice Core Drill Site Identification in East
692 Antarctica: Development and First Results, *IEEE Journal of Selected Topics in Applied Earth
693 Observations and Remote Sensing*, 13, 4836-4847, 2020.
- 694 40. Saito, F. and A. Abe-Ouchi.: Thermal structure of Dome Fuji and east Dronning Maud Land,
695 Antarctica, simulated by a three-dimensional ice-sheet model, *Ann. Glaciol.*, 39, 433–438, doi:
696 10.3189/172756404781814258, 2004.
- 697 41. Saito, F., and Abe-Ouchi, A.: Modelled response of the volume and thickness of the Antarctic ice
698 sheet to the advance of the grounded area, *Ann. of Glaciol.*, 51, 41-48, doi:
699 10.3189/172756410791392808, 2010.
- 700 42. Saito, F., Obase, T., and Abe-Ouchi, A.: Implementation of the RCIP scheme and its performance
701 for 1-D age computations in ice-sheet models, *Geosci. Model Dev.*, 13, 5875–5896,
702 doi:10.5194/gmd-13-5875-2020, 2020.
- 703 43. Saruya, T., Fujita, S., Iizuka, Y., Miyamoto, A., Ohno, H., Hori, A., Shigeyama, W., Hirabayashi,
704 M., and Goto-Azuma, K.: Development of crystal orientation fabric in the Dome Fuji ice core in
705 East Antarctica: implications for the deformation regime in ice sheets, *The Cryosphere*, 16, 2985–
706 3003, <https://doi.org/10.5194/tc-16-2985-2022>, 2022.
- 707 44. Seddik, H., Greve, R., Zwinger, T., and Placidi, L.: A full Stokes ice flow model for the vicinity
708 of Dome Fuji, Antarctica, with induced anisotropy and fabric evolution, *The Cryosphere*, 5, 495–
709 508, doi:10.5194/tc-5-495-2011, 2011.
- 710 45. Sun, B., Moore, J. C., Zwinger, T., Zhao, L., Steinhage, D., Tang, X., Zhang, D., Cui, X., and
711 Martín, C.: How old is the ice beneath Dome A, Antarctica?, *The Cryosphere*, 8, 1121–1128,
712 doi:10.5194/tc-8-1121-2014, 2014.
- 713 46. Sutter, J., Fischer, H., Grosfeld, K., Karlsson, N. B., Kleiner, T., Van Liefferinge, B., and Eisen,
714 O.: Modelling the Antarctic Ice Sheet across the mid-Pleistocene transition – implications for
715 Oldest Ice, *The Cryosphere*, 13, 2023–2041, <https://doi.org/10.5194/tc-13-2023-2019>, 2019.
- 716 47. Sutter, J., Fischer, H., and Eisen, O.: Investigating the internal structure of the Antarctic ice sheet:
717 the utility of isochrones for spatiotemporal ice-sheet model calibration, *The Cryosphere*, 15, 3839–
718 3860, <https://doi.org/10.5194/tc-15-3839-2021>, 2021.
- 719 48. Talalay, P., Li, Y., Augustin, L., Clow, G. D., Hong, J., Lefebvre, E., Markov, A., Motoyama, H.,
720 and Ritz, C.: Geothermal heat flux from measured temperature profiles in deep ice boreholes in
721 Antarctica, *The Cryosphere*, 14, 4021–4037, <https://doi.org/10.5194/tc-14-4021-2020>, 2020.
- 722 49. Tsutaki, S., Fujita, S., Kawamura, K., Abe-Ouchi, A., Fukui, K., Motoyama, H., Hoshina, Y.,
723 Nakazawa, F., Obase, T., Ohno, H., Oyabu, I., Saito, F., Sugiura, K., and Suzuki, T.: High-
724 resolution subglacial topography around Dome Fuji, Antarctica, based on ground-based radar
725 surveys conducted over 30 years, *The Cryosphere*, 16, 2967-2983, doi: 10.5194/tc-16-2967-2022,
726 2022
- 727 50. Uemura, R., Motoyama, H., Masson-Delmotte, V., Jouzel, J., Kawamura, K., Goto-Azuma, K.,
728 Fujita, S., Kuramoto, T., Hirabayashi, M., Miyake, T., Ohno, H., Fujita, K., Abe-Ouchi, A., Iizuka,
729 Y., Horikawa, S., Igarashi, M., Suzuki, K., Suzuki, T., and Fujii, Y.: Asynchrony between
730 Antarctic temperature and CO₂ associated with obliquity over the past 720,000 years, *Nat.*
731 *Commun.*, 9, 961, doi:10.1038/s41467-018-03328-3, 2018.



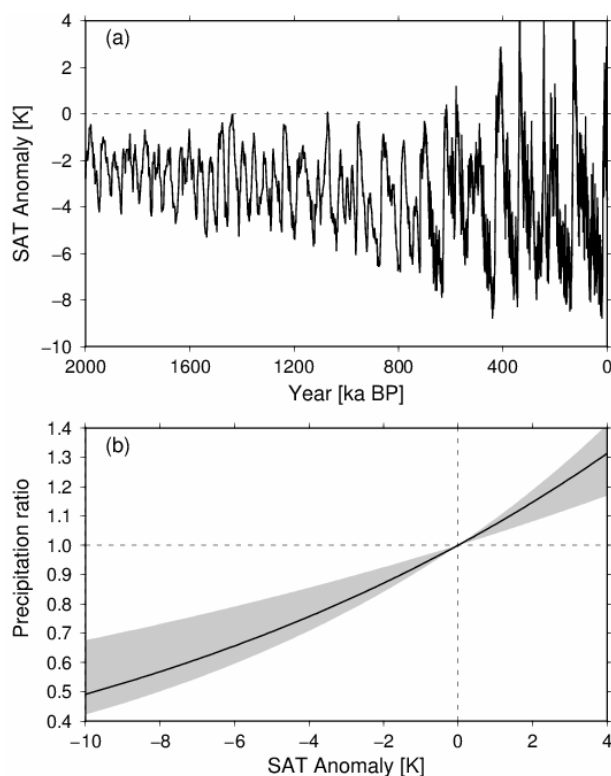
- 732 51. Van Liefferinge, B. and Pattyn, F.: Using ice-flow models to evaluate potential sites of million
733 year-old ice in Antarctica, *Clim. Past*, 9, 2335–2345, doi:10.5194/cp-9-2335-2013, 2013.
- 734 52. Van Liefferinge, B., Pattyn, F., Cavitte, M. G. P., Karlsson, N. B., Young, D. A., Sutter, J., and
735 Eisen, O.: Promising Oldest Ice sites in East Antarctica based on thermodynamical modelling, *The*
736 *Cryosphere*, 12, 2773–2787, doi:10.5194/tc-12-2773-2018, 2018.
- 737 53. Van Liefferinge, B., Taylor, D., Tsutaki, S., Fujita, S., Gogineni, P., Kawamura, K., et al., Surface
738 mass balance controlled by local surface slope in inland Antarctica: Implications for ice-sheet
739 mass balance and Oldest Ice delineation in Dome Fuji. *Geophysical Research Letters*, 48,
740 e2021GL094966. doi:10.1029/2021GL094966, 2021.
- 741 54. Veres, D., L. Bazin, A. Landais, H. Toyé Mahamadou Kele, B. Lemieux-Dudon, F. Parrenin, P.
742 Martinerie, E. Blayo, T. Blunier, E. Capron, J. Chappellaz, S.O. Rasmussen, M. Severi, A.
743 Svensson, B. Vinther, and E.W. Wolff, The Antarctic ice core chronology (AICC2012): an
744 optimized multi-parameter and multi-site dating approach for the last 120 thousand years, *Climate*
745 *of the Past*, 9, 1733-1748, doi: 10.5194/cp-9-1733-2013, 2013.
- 746 55. Yamanouchi, T., Hirasawa, N., Hayashi, M., Takahashi, S., Kaneto S.: Meteorological
747 characteristics of Antarctic inland station, Dome Fuji, *Memoirs of National Institute of Polar*
748 *Research*. Special issue 57, 94-104, 2003
- 749 56. Young, D. A., Roberts, J. L., Ritz, C., Frezzotti, M., Quartini, E., Cavitte, M. G. P., Tozer, C. R.,
750 Steinhage, D., Urbini, S., Corr, H. F. J., van Ommen, T., and Blankenship, D. D.: High-resolution
751 boundary conditions of an old ice target near Dome C, Antarctica, *The Cryosphere*, 11, 1897–
752 1911, <https://doi.org/10.5194/tc-11-1897-2017>, 2017
- 753 57. Zhao, L., Moore, J. C., Sun, B., Tang, X., and Guo, X.: Where is the 1-million-year-old ice at
754 Dome A?, *The Cryosphere*, 12, 1651–1663, doi:10.5194/tc-12-1651-2018, 2018.
- 755



756 Fig. 1: (a) Map of Antarctica. The contours (every 500 m) indicate the surface elevation, and colors
757 indicate ice thickness, using BEDMAP2 (Fretwell et al., 2013). The square indicates the location of
758 the inset shown in (b). (b) Enlarged view near DF (Dome Fuji). The triangle indicates the location of
759 the DF ice core site, and the diamond indicates the NDF site.
760



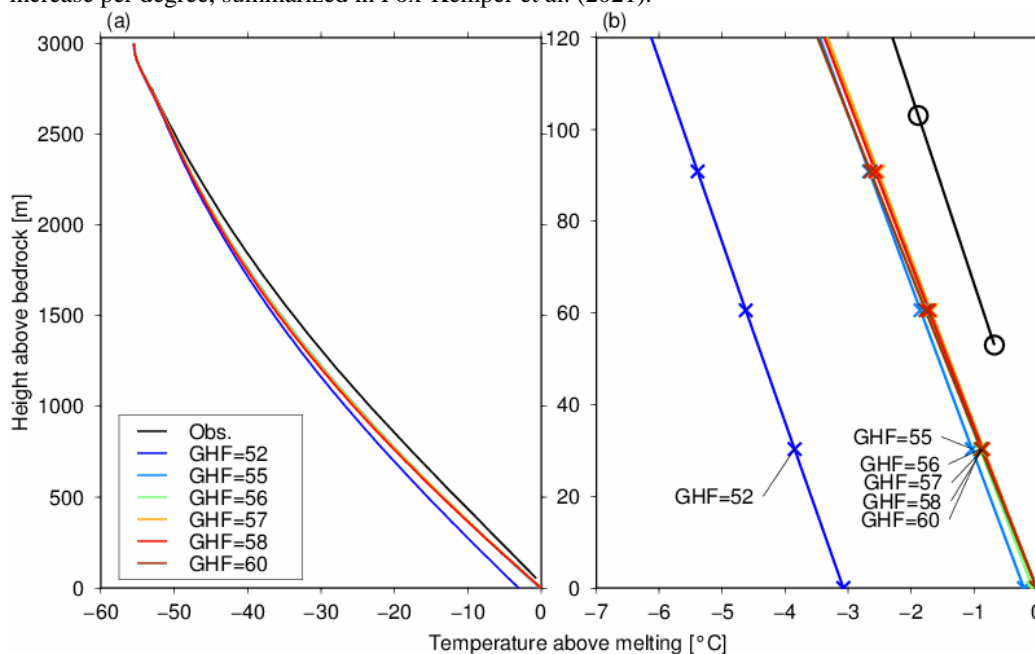
761
 762 Fig. 2: (a) Normalized vertical velocity profiles adopted from Equation [1] with different p parameters.
 763 The dashed black line (HF13) indicates the vertical velocity profile used in Fischer et al. (2013) with
 764 $m = 0.5$. (b) Enlarged view near the bottom of the ice column (see black rectangle in (a)).
 765
 766



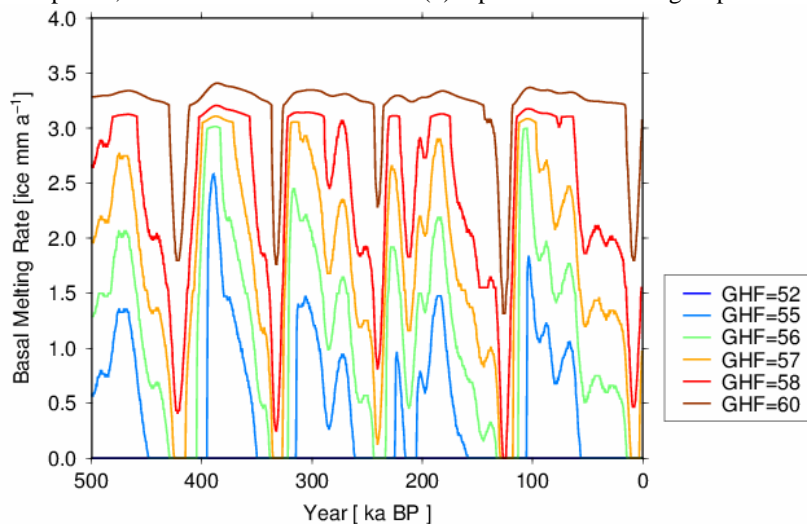
767
 768 Fig. 3: Glacial cycle forcing used in the present study. (a) Surface air temperature (SAT) anomaly from



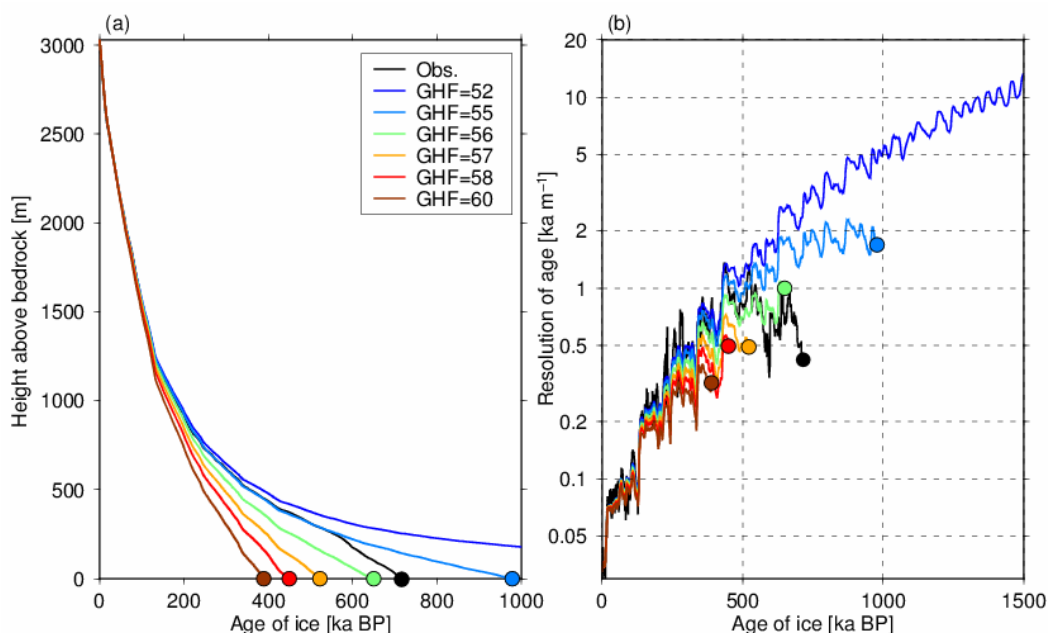
769 the present day for the last 2 Ma. (b) Relationship between SAT anomaly and precipitation ratio. The
 770 black line corresponds to the one used in the present study; the gray shading indicates a 4%–9%
 771 increase per degree, summarized in Fox-Kemper et al. (2021).



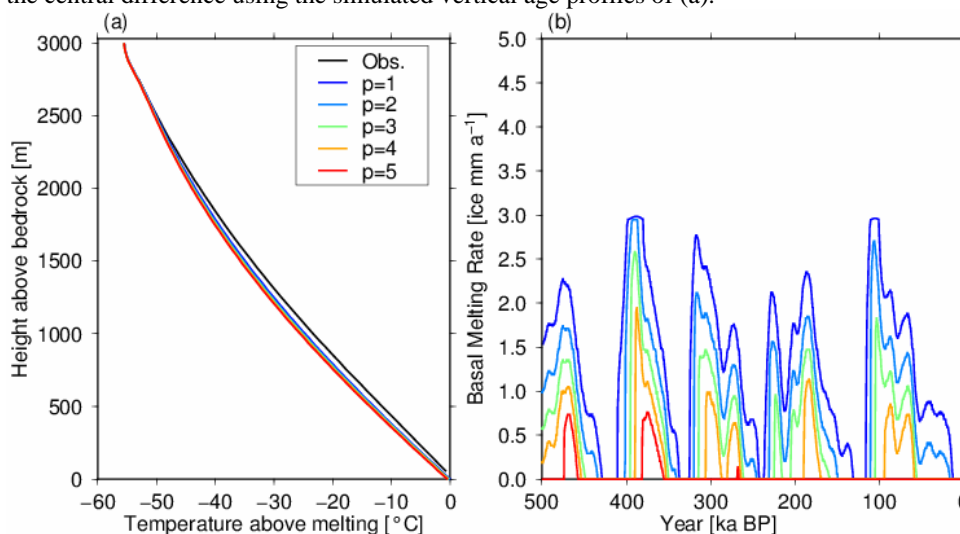
772
 773 Fig. 4: Simulated vertical temperature profiles under the DF configuration (Table 1) with different
 774 geothermal heat fluxes (GHF; units are mW m^{-2}). (a) Simulated temperature profiles at 0 ka (end of
 775 the simulation) from the surface to the base. (b) Close-up of (a) for the bottom 120 m of the ice column.
 776 The black lines represent the measured temperature profiles and the black circles in (b) indicate the
 777 location of data points, while the colored crosses in (b) represent the model grid points.



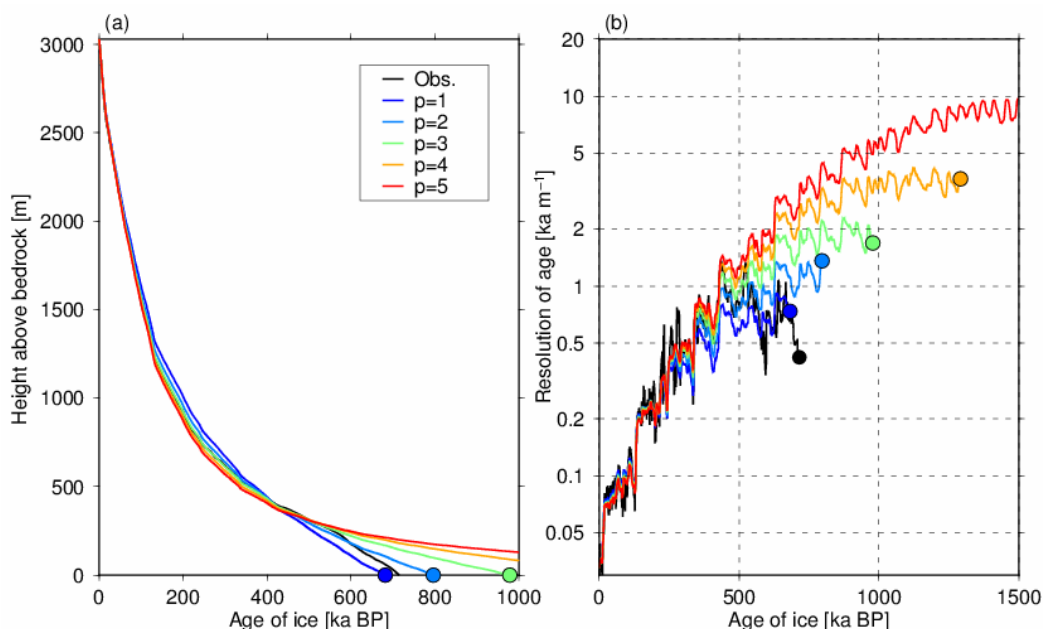
778
 779 Fig. 5: Time series of the simulated basal melting rates of the last 500 ka under the DF configuration
 780 (Table 1) with different geothermal heat fluxes (GHF; units are mW m^{-2}).



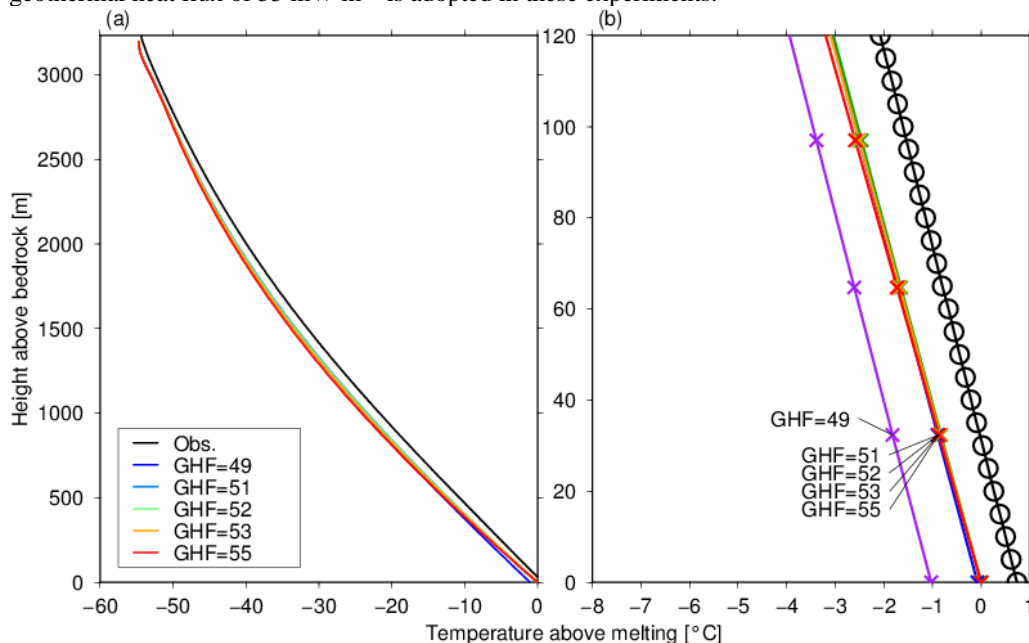
781
 782 Fig. 6: Simulated vertical ice age profiles under the DF configuration (Table 1) with different
 783 geothermal heat fluxes (GHF; units are mW m^{-2}). (a) Vertical age profiles at present (0 ka). The black
 784 line represents the reconstructed depth–age profile based on the AICC2012 chronology (Kawamura
 785 et al., 2017). The circles indicate the bottom of the ice. (b) Vertical resolution of ice age, calculated by
 786 the central difference using the simulated vertical age profiles of (a).



787
 788 Fig. 7: Simulated vertical temperature profiles and basal melting rates under the DF configuration
 789 (Table 1) with different p parameters. (a) Simulated temperature profiles at present (0 ka) from the
 790 surface to the base. (b) Time series of basal melting rates over the last 500 ka. A geothermal heat flux
 791 of 55 mW m^{-2} is adopted in these experiments.



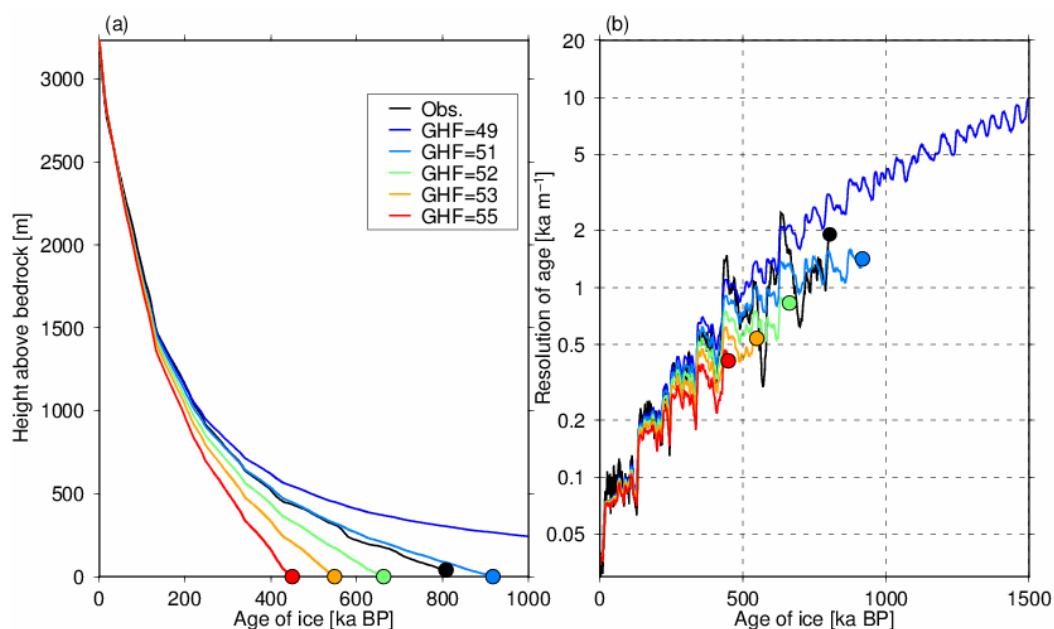
792 Fig. 8: Same as Fig. 6, with different p parameters. (a) Simulated age profiles at present (0 ka) from
 793 the surface to the base. (b) Vertical resolution of ice age. The circles indicate the bottom of the ice. A
 794 geothermal heat flux of 55 mW m^{-2} is adopted in these experiments.
 795



796 Fig. 9: Same as Fig. 4, but under the EDC configuration (Table 1) with different geothermal heat
 797 fluxes (GHF; units are mW m^{-2}). The black lines represent the measured temperature profiles and the
 798 black circles in (b) indicate the location of data points, while the colored crosses in (b) represent the
 799 model grid points.
 800

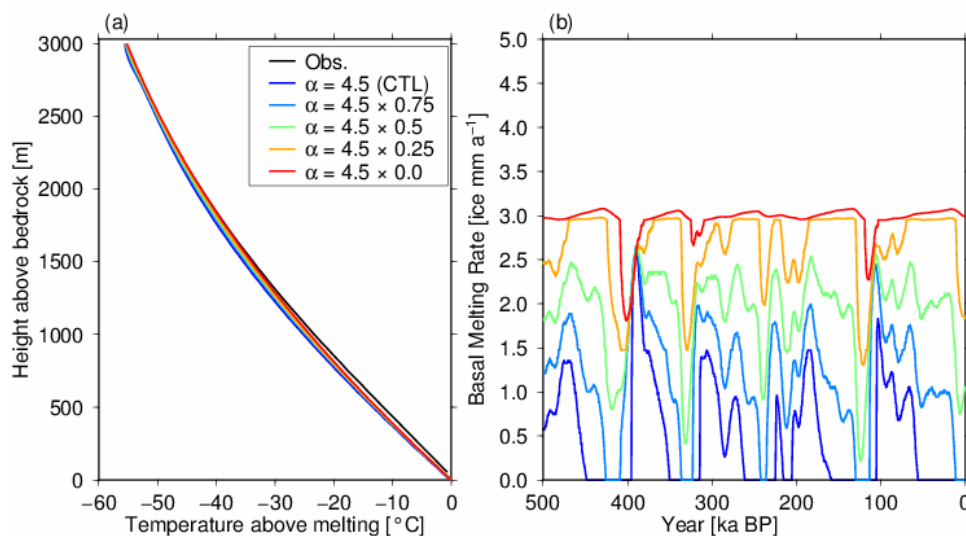


801
 802



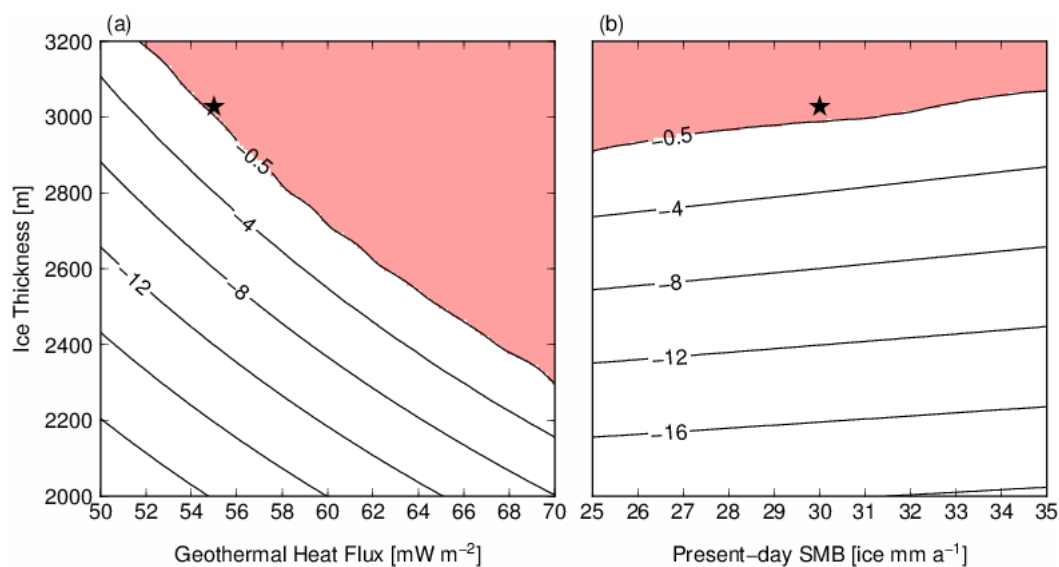
803
 804
 805
 806

Fig. 10: Same as Fig. 6, but results under the EDC configuration (Table 1). The AICC2012 chronology (Veres et al., 2013) is used in this figure for the observed depth–age profile.

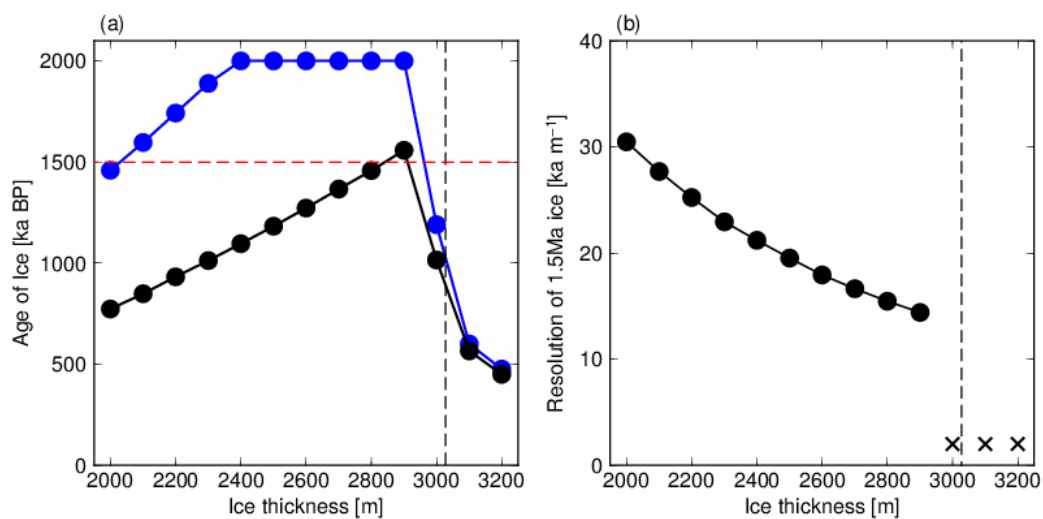


807
 808
 809
 810
 811
 812
 813

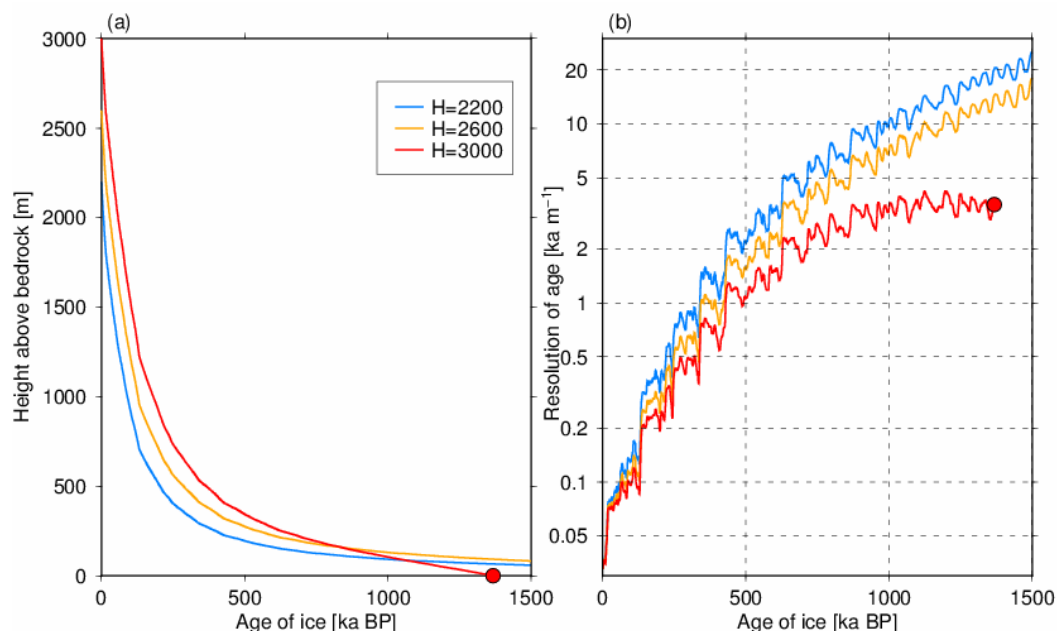
Fig. 11: Simulated vertical temperature profiles and basal melting rates under the DF configuration (Table 1), using different temperature amplitudes over glacial cycles in Equation 8. A combination of $p = 3$ and $\text{GHF} = 55 \text{ mW m}^{-2}$ is adopted in these experiments. (a) Simulated temperature profiles at present (0 ka) from the surface to the base. (b) Basal melting rates of the last 500 ka. The dark blue lines are the same as the green line of Fig. 4.



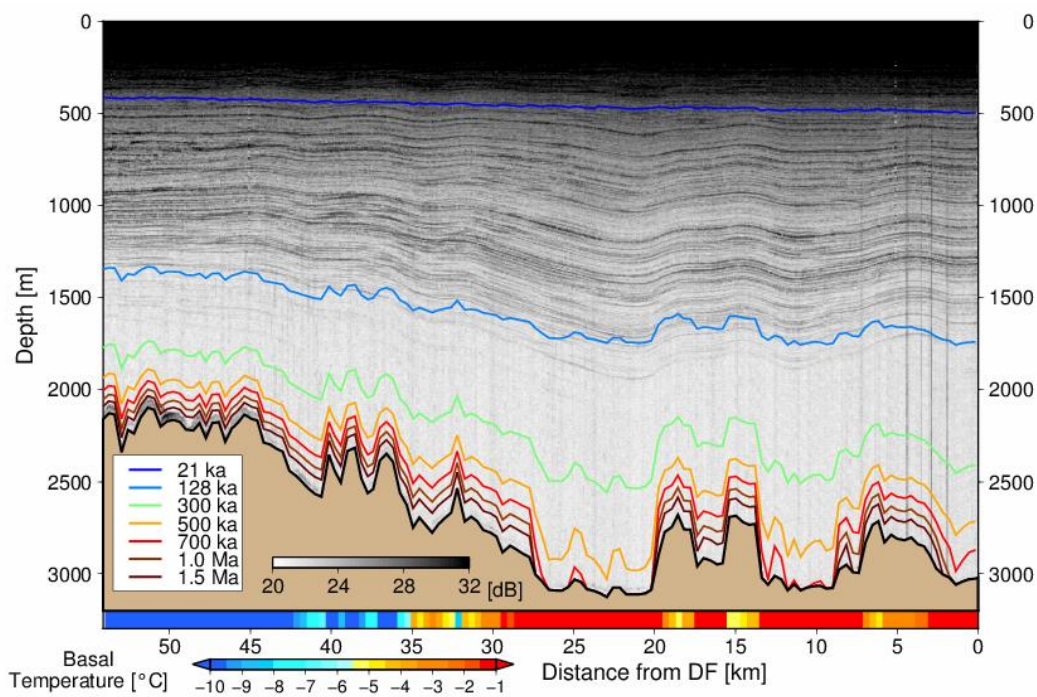
814
 815 Fig. 12: Simulated basal temperature at the present day with combinations of ice thickness, geothermal
 816 heat flux, and present-day SMB. (a) Red shading indicates a basal temperature -0.5 °C below the
 817 pressure-melting point. (b) Basal temperature at the present day with $\text{GHF} = 55\text{ mW m}^{-2}$. The black
 818 star represents the condition at the DF ice core ($H = 3028\text{ m}$, $\text{SMB} = 30\text{ ice mm a}^{-1}$), with a calibrated
 819 geothermal heat flux (55 mW m^{-2}).
 820



821
 822 Fig. 13: Results with different ice thicknesses. (a) The black and blue lines indicate the simulated age of the ice at 100 and 50 m above the bedrock, respectively. The vertical dashed line ($H = 3028\text{ m}$)
 823 indicates the condition at DF, and the horizontal red dashed line indicates the age of 1.5 Ma. Note that
 824 an age of 2 Ma is the limit of the experiments. (b) The vertical axis indicates the resolution of the ice
 825 age (ka m^{-1}) at 1.5 Ma BP. The crosses indicate that the 1.5 Ma age of ice does not exist under these
 826 conditions.
 827



828
 829 Fig. 14: Results with different ice thicknesses (2200, 2600, and 3000 m) with calibrated geothermal
 830 heat flux and SMB (55 mW m^{-2} , 30 ice mm a^{-1}) at DF. (a) Vertical age profiles (the circle on the H =
 831 3000 m case indicates the bottom of the ice) at present (0 ka). (b) Vertical resolution of the ice age.
 832



833
 834 Fig. 15: Results of the experiments overlaid with the observed radargram for the DF–NDF transect.



835 The horizontal axis indicates the distance from DF (km), and the vertical axis indicates the depth from
836 the surface (m). The gray coloring indicates the reflection intensity from the ground radar surveys, and
837 the color contours indicate the simulated age of the ice using the 1-D model. The bottom color bar
838 indicates the simulated basal temperature (relative to the melting point) at the present-day.